

1 **Magnetospheric chaos and dynamical complexity response during storm time disturbance**

2 Irewola Aaron Oludehinwa<sup>1</sup>, Olasunkanmi Isaac Olusola<sup>1</sup>, Olawale Segun Bolaji<sup>1,2</sup>, Olumide  
3 Olayinka Odeyemi<sup>1</sup>, Abdullahi Ndzi Njah<sup>1</sup>

4 <sup>1</sup>Department of Physics, University of Lagos, Nigeria

5 <sup>2</sup>Department of Physics, University of Tasmania, Australia

6 **Abstract**

7 In this study, we examine the magnetospheric chaos and dynamical complexity response to the  
8 disturbance storm time ( $D_{st}$ ) and solar wind electric field ( $VB_s$ ) during different categories of  
9 geomagnetic storm (minor, moderate and major geomagnetic storm). The time series data of the  
10  $D_{st}$  and  $VB_s$  are analyzed for the period of nine years using nonlinear dynamics tools (Maximal  
11 Lyapunov Exponent, MLE, Approximate Entropy, ApEn and Delay Vector Variance, DVV). We  
12 found a significant trend between each nonlinear parameter and the categories of geomagnetic  
13 storm. The MLE and ApEn values of the  $D_{st}$  indicate that chaotic and dynamical complexity  
14 responses are high during minor geomagnetic storms, reduce at moderate geomagnetic storms and  
15 decline further during major geomagnetic storms. However, the MLE and ApEn values obtained  
16 from  $VB_s$  indicate that chaotic and dynamical complexity response are high with no significant  
17 difference between the periods that are associated with minor, moderate and major geomagnetic  
18 storms. The test for nonlinearity in the  $D_{st}$  time series during major geomagnetic storm reveals the  
19 strongest nonlinearity features. Based on these findings, the dynamical features obtained in the  
20  $VB_s$  as input and  $D_{st}$  as output of the magnetospheric system suggest that the magnetospheric  
21 dynamics is nonlinear and the solar wind dynamics is consistently stochastic in nature.

22 **Keywords:**  $D_{st}$  signals, Solar wind electric field ( $VB_s$ ) signals, Geomagnetic storm, Chaotic  
23 behaviour, Dynamical complexity, Nonlinearity.

25 **1.0 Introduction**

26 The response of chaos and dynamical complexity behaviour with respect to magnetospheric  
27 dynamics varies. This is due to changes in the interplanetary electric fields imposed on the  
28 magnetopause and those penetrating the inner magnetosphere and sustaining convection thereby  
29 initiating geomagnetic storm (Pavlos et al. 1992). A prolonged southward turning of interplanetary  
30 magnetic field (IMF, $B_z$ ), which indicates that solar wind-magnetosphere coupling is in-progress  
31 was confirmed on many occasions **for which** such geomagnetic storm was **driven by** Corotating  
32 **Interaction Regions (CIRs)**, or by the sheath preceding an interplanetary coronal mass ejection  
33 (**ICME**) or by a combination of the sheath and an ICME magnetic cloud (Russell et al. 1974;  
34 Burton et al. 1975; Gonzalez and Tsurutani, 1987; Tsurutani et al. 1988; Cowley, 1995; Tsutomu,  
35 2002; Yurchyshyn et al. 2004; Kozyra et al. 2006; Echer et al. 2008; Meng et al. 2019; Tsurutani  
36 et al. 2020). Notably, the introduction of Disturbance Storm Time ( $D_{st}$ ) index (Sugiura, 1964;  
37 Sugiura and Kamei, 1991) unveil the quantitative measure of the total energy of the ring current  
38 particles. Therefore, the  $D_{st}$  index remains one of the most popular global indicators that can  
39 precisely reveal the severity of a geomagnetic storm (Dessler and Parker, 1959).

40 The  $D_{st}$  fluctuations exhibit different signatures for different categories of geomagnetic storm.  
41 Ordinarily, one can easily anticipate that fluctuations in a  $D_{st}$  signal appear chaotic and complex.  
42 These may arise from the changes in the interplanetary electric fields driven by the solar wind-  
43 magnetospheric coupling processes. At different categories of geomagnetic storm, fluctuations in  
44 the  $D_{st}$  signals differ (Oludehinwa et al. 2018). One obvious reason is that as the intensity of the  
45 geomagnetic storm increases, the fluctuation behaviour in the  $D_{st}$  signal becomes more complex  
46 and nonlinear in nature. **It has** been established that the electrodynamic response of the  
47 magnetosphere to solar wind **driver** are non-autonomous in nature (Price and Prichard, 1993; Price

48 et al. 1994; Johnson and Wings, 2005). Therefore, the chaotic analysis of the magnetospheric time  
49 series must be related to the concept of input-output dynamical process. Consequently, it is  
50 necessary to examine the chaotic behaviour of the solar wind electric field ( $VB_s$ ) as input signals  
51 and the magnetospheric activity index ( $D_{st}$ ) as output during different categories of geomagnetic  
52 storms.

53 Several works have been presented on the chaotic and dynamical complexity behaviour of the  
54 magnetospheric dynamics based on autonomous concept, i.e using the time series data of  
55 magnetospheric activity alone such as auroral electrojet (AE), **Amplitude Lower (AL)** and  $D_{st}$   
56 index (Vassiliadis et al. 1990; Baker and Klimas, 1990; Vassiliadis et al. 1991; Shan et al. 1991;  
57 Pavlos et al. 1994; Klimas et al. 1996; Valdivia et al. 2005; Mendes et al. 2017; Consolini, 2018).  
58 They found evidence of low-dimensional chaos in the magnetospheric dynamics. For instance, the  
59 report by Vassiliadis et al. (1991) shows that the computation of Lyapunov exponent for AL index  
60 time series gives a positive value of Lyapunov exponent indicating the presence of chaos in the  
61 magnetospheric dynamics. Unnikrishnan, (2008) studied the deterministic chaotic behaviour in the  
62 magnetospheric dynamics under various physical conditions using AE index time series and found  
63 that the seasonal mean value of Lyapunov exponent in winter season during quiet periods ( $0.7 \pm$   
64  $0.11 \text{ min}^{-1}$ ) is higher than that of the stormy periods ( $0.36 \pm 0.09 \text{ min}^{-1}$ ). Balasis et al. (2006)  
65 examined the magnetospheric dynamics in the  $D_{st}$  index time series from pre-magnetic storm to  
66 magnetic storm period using fractal dynamics. They found that the transition from anti-persistent  
67 to persistent behaviour indicates that the occurrence of an intense geomagnetic storm is imminent.  
68 Balasis et al. (2009) further reveal the dynamical complexity behaviour in the magnetospheric  
69 dynamics using various entropy measures. They reported a significant decrease in dynamical  
70 complexity and an accession of persistency in the  $D_{st}$  time series as the magnetic storm

71 approaches. Recently, Oludehinwa et al. (2018) examined the nonlinearity effects in  $D_{st}$  signals  
72 during minor, moderate and major geomagnetic storm using recurrence plot and recurrence  
73 quantification analysis. They found that the dynamics of the  $D_{st}$  signal is stochastic during minor  
74 geomagnetic storm periods and deterministic as the geomagnetic storm increases.

75 Also, studies describing the solar wind and magnetosphere as non-autonomous system have been  
76 extensively investigated. Price et al. (1994) examine the nonlinear input-output analysis of AL  
77 index and different combinations of interplanetary magnetic field (IMF) with solar wind  
78 parameters as input function. They found that only a few of the input combinations show any  
79 evidence whatsoever for nonlinear coupling between the input and output for the interval  
80 investigated. Pavlos et al. (1999) **presented** further evidence of magnetospheric chaos. They  
81 compared the observational behaviour of the magnetospheric system with the results obtained by  
82 analyzing different types of stochastic and deterministic input-output systems and **asserted** that a  
83 low dimensional chaos is evident in magnetospheric dynamics. Devi et al. (2013) studied the  
84 magnetospheric dynamics using AL index with the southward component of IMF, (Bz) and  
85 observed that the magnetosphere and turbulent solar wind have values corresponding to nonlinear  
86 dynamical system with chaotic behaviour. The modeling and forecasting approach have been  
87 applied to magnetospheric time series using nonlinear models (Valdivia et al. 1996; Vassiliadis et  
88 al. 1999; Vassiliadis, 2006; Balikhin et al. 2010). These efforts have improved our understanding  
89 with regards to the facts that nonlinear dynamics can reveal some hidden dynamical information  
90 in the observational time series. In addition to these nonlinear effects in  $D_{st}$  signals, a measure of  
91 the exponential divergence and convergence within the trajectories of a phase space known as  
92 **Maximal Lyapunov Exponent (MLE)**, which **has the potential to depict** the chaotic behavior in the  
93  $D_{st}$  and  $VB_s$  time series during a minor, moderate and major geomagnetic storm have not been

94 investigated. In addition, to the best of our knowledge, computation of Approximate Entropy  
95 (ApEn) that depicts the dynamical complexity behaviour during different categories of  
96 geomagnetic storm has not been reported in the literature. The test for nonlinearity through delay  
97 vector variance (DVV) analysis that establishes the degree at which nonlinearity response in  $D_{st}$   
98 time series during minor, moderate and major geomagnetic storms is not well known. It is worth  
99 to note that understanding the dynamical characteristics in the  $D_{st}$  and  $VB_s$  signals at different  
100 categories of geomagnetic storms will provide useful diagnostic information to different conditions  
101 of space weather **phenomenon**. Consequently, this study attempts to carry out comprehensive  
102 numerical analysis to unfold the chaotic and dynamical complexity behaviour in the  $D_{st}$  and  $VB_s$   
103 signals during minor, moderate and major geomagnetic storm. In section 2, our methods of data  
104 acquisition are described. Also, the nonlinear analysis that we employed in this investigation are  
105 detailed. In section 3, we unveiled our results and engage the discussion of results in section 5.

## 106 **2.0 Description of the Data and Nonlinear Dynamics**

107 The  $D_{st}$  index is **derived by measurements from** ground-based magnetic stations at low-latitudes  
108 observatories around the world and **depicts mainly the variation of the ring current, as well as the**  
109 **Chapman-Ferraro Magnetopause currents, and tail currents to a lesser extent** (Sugiura, 1964; Love  
110 and Gannon, 2009). Due to its global nature,  $D_{st}$  time series provides a measure of how intense a  
111 geomagnetic storm was (Dessel and Parker, 1959). In this study, we considered  $D_{st}$  data for the  
112 period of nine years from January to December between 2008 and 2016 which were downloaded  
113 from the World Data Centre for Geomagnetism, Kyoto, Japan (<http://wdc.kugi-kyoto-u.ac.jp/Dstae/index.html>). **The sampling time of  $D_{st}$  and  $VB_s$  time series data was 1-hour.** We use  
115 the classification of geomagnetic storms as proposed by Gonzalez et al. (1994) such that  $D_{st}$  index  
116 value in the ranges  $0 \leq Dst \leq -50nT$ ,  $-50nT \leq Dst \leq -100nT$ ,  $-100nT \leq Dst \leq -250nT$

117 are classified as minor, moderate and major geomagnetic storms respectively **and each month is**  
118 **being classified based on its minimum Dst value.** The solar wind electric field ( $VB_s$ ) data are  
119 archived from the National Aeronautics and Space Administration, Space Physics Facility  
120 (<http://omniweb.gsfc.nasa.gov>). It is well known that the dynamics of the solar wind contribute to  
121 the driving of the magnetosphere (Burton et al. 1975). Furthermore, we took the solar wind electric  
122 field ( $VB_s$ ) as the input **signal** (Price and Prichard, 1993; Price et al. 1994). The  $VB_s$  was  
123 categorized according to the periods of minor, moderate and major geomagnetic storm. Then, the  
124  $D_{st}$  and  $VB_s$  time series were subjected to a variety of nonlinear analytical tools explained as  
125 follow:

## 126 **2.1 Phase Space Reconstruction and Observational time series**

127 An observational time series can be defined as a sequence of scalar measurements of some  
128 quantity, which is a function of the current state of the system taken at multiples of a fixed sampling  
129 time. In nonlinear dynamics, the first step in analyzing an observational time series data is to  
130 reconstruct an appropriate state space of the system. Takens, (1981) and Mane, (1981) stated that  
131 one time series or a few simultaneous time series are converted to a sequence of vectors. This  
132 reconstructed phase space has all the dynamical characteristic of the real phase space provided the  
133 time delay and embedding dimension are properly specified.

$$134 \quad X(t) = [x(t), x(t + \tau), x(t + 2\tau), \dots, x(t + (m - 1)\tau)]^T \quad (1)$$

135 Where  $X(t)$  is the reconstructed phase space,  $x(t)$  is the original time series data,  $\tau$  is the time  
136 delay and  $m$  is the embedding dimension. An appropriate choice of  $\tau$  and  $m$  are needed for the  
137 reconstruction phase space which is determined by average mutual information and false nearest  
138 neighbour respectively.

139 **2.2 Average Mutual Information (AMI)**

140 The method of Average Mutual Information (AMI) is one of the nonlinear techniques used to  
141 determine the optimal time delay ( $\tau$ ) required for phase space reconstruction in observational time  
142 series. The time delay mutual information was proposed by Fraser and Swinney, (1986) instead of  
143 autocorrelation function. This method takes into account nonlinear correlations within the time  
144 series data. It measures how much information can be predicted about one time series point, given  
145 full information about the other. For instance, the mutual information between  $x_i$  and  $x_{(i+\tau)}$   
146 quantifies the information in state  $x_{(i+\tau)}$  under the assumption that information at the state  $x_i$  is  
147 known. The AMI for a time series,  $x(t_i)$ ,  $i = 1, 2, \dots, N$  is calculated as:

148 
$$I(T) = \sum_{x(t_i), x(t_i+T)} P(x(t_i), x(t_i + T)) \times \log_2 \left[ \frac{P(x(t_i), x(t_i + T))}{P(x(t_i)) P(x(t_i + T))} \right] \quad (2)$$

149 Where  $x(t_i)$  is the  $i$ th element of the time series,  $T = k\Delta t$  ( $k = 1, 2, \dots, k_{max}$ ),  $P(x(t_i))$  is the  
150 probability density at  $x(t_i)$ ,  $P(x(t_i), x(t_i + T))$  is the joint probability density at the pair  
151  $x(t_i), x(t_i + T)$ . The time delay ( $\tau$ ) of the first minimum of AMI is chosen as optimal time delay  
152 (Fraser and Swinney, 1986). Therefore, the AMI was applied to the  $D_{st}$  and  $VB_s$  time series and  
153 the plot of AMI against time delay is shown in Figure (3). We notice that the AMI showed the first  
154 local minimum at roughly ( $\tau = 15hr$ ). Furthermore, the values of  $\tau$  near this value of ( $\sim 15hr$ )  
155 maintain constancy for both VBs and  $D_{st}$ . In the analysis ( $\tau = 15hr$ ) was used as the optimal  
156 time delay for the computation of maximal Lyapunov exponent.

157

158

159

160 **2.3 False Nearest Neighbour (FNN)**

161 In determining the optimal choice of embedding dimension( $m$ ), the false nearest neighbour  
162 method was used in the study. It was suggested by Kennel et al. (1992). The concept is based on  
163 how the number of neighbours of a point along a signal trajectory changes with increasing  
164 embedding dimension. With increasing embedding dimension, the false neighbour will no longer  
165 be neighbours, therefore by examining how the number of neighbours changes as a function of  
166 dimension, an appropriate embedding dimension can be determined. For instance, suppose we  
167 have a one-dimensional time series. We can construct a time series  $y(t)$  of  $D$ -dimensional points  
168 from the original one-dimensional time series  $x(t)$  as follows:

169 
$$y(t) = (x(t), x(t + \tau), \dots, x(t + (D - 1)\tau)) \quad (3)$$

170 Where  $\tau$  and  $D$  are time delay and embedding dimension. Using the formular from Kennel et al.  
171 (1992); Wallot and Monster, (2018). If we have a  $D$ -dimensional phase space and denote the  $r$ th  
172 nearest neighbour of a coordinate vector  $y(t)$  by  $y^{(r)}(t)$ , then the square of the Euclidean distance  
173 between  $y(t)$  and the  $r$ th nearest neighbor is:

174 
$$R_D^2(t, r) = \sum_{k=0}^{D-1} [x(t + k\tau) - x^{(r)}(t + k\tau)]^2 \quad (4)$$

175 Now applying the logic outlined above, we can go from a  $D$ -dimensional phase space to  $(D + 1)$   
176 dimensional phase space by time-delay embedding, adding a new coordinate to  $y(t)$ , and ask what  
177 is the squared distance between  $y(t)$  and the same  $r$ th nearest neighbour:

178 
$$R_{D+1}^2(t, r) = R_D^2(t, r) + [x(t + D\tau) - x^{(r)}(t + D\tau)]^2 \quad (5)$$

179 As explained above, if the one-dimensional time series is already properly embedded in  $D$   
180 dimensions, then the distance  $R$  between  $y(t)$  and the  $r$ th nearest neighbour should not  
181 appreciably change by some distance criterion  $R_{tol}$  (i.e  $R < R_{tol}$ ). Moreover, the distance of the  
182 nearest neighbour when embedded into the next higher dimension relative to the size of the  
183 attractor should be less than some criterion  $A_{tol}$  (i.e  $R_{D+1} < A_{tol}$ ). Doing this for the nearest  
184 neighbour of each coordinate will result on many false nearest neighbours when embedding is  
185 insufficient or in few (or no) false neighbours when embedding is sufficient. In the analysis, the  
186 FNN was applied to the  $D_{st}$  and  $VB_s$  time series to detect the optimal value of embedding  
187 dimension( $m$ ). Figure (4) shows a sample plot of the percentage of false nearest neighbour against  
188 embedding dimension in one of the months under investigation (other months show similar results,  
189 thus for brevity we depict only one of the results). We notice that the false nearest neighbor attains  
190 its minimum value at  $m \geq 5$  indicating that embedding dimension ( $m$ ) from  $m \geq 5$  are optimal  
191 values. Therefore,  $m = 5$  was used for the computation of maximal Lyapunov exponent.

## 192 **2.4 Maximal Lyapunov Exponent (MLE)**

193 The Maximal Lyapunov Exponent (MLE) is one of the most popular nonlinear dynamics tool used  
194 for detecting chaotic behaviour in a time series data. It describes how small changes in the state of  
195 a system grow at an exponential rate and eventually dominate the behaviour. An important  
196 indication of chaotic behavior of a dissipative deterministic system is the existence of a positive  
197 Lyapunov Exponent. A positive MLE signifies divergence of trajectories in one direction or  
198 expansion of an initial volume in this direction. On the other hand, a negative MLE exponent  
199 implies convergence of trajectories or contraction of volume along another direction. The  
200 algorithm proposed by Wolf et al. (1985) for estimating MLE is employed to compute the chaotic  
201 behavior of the  $D_{st}$  and  $VB_s$  time series at minor, moderate and major geomagnetic storm. Other

202 methods of determining MLE includes Rosenstein's method, Kantz's method and so on. In this  
203 study, the MLE at minor, moderate and major geomagnetic storms periods was computed with  
204  $m = 5$  and  $\tau = 15\text{hr}$  as shown in figures (5 & 6-bar plots) for  $D_{st}$  and  $VB_S$ . The calculation of  
205 MLE is explained as follows: given a sequence of vector  $x(t)$ , an  $m$ -dimensional phase space is  
206 formed from the observational time series through embedding theorem as

207 
$$\{x(t), x(t + \tau), \dots, x(t + (m - 1)\tau)\} \quad (6)$$

208 Where  $m$  and  $\tau$  are as defined earlier, after reconstructing the observational time series, the  
209 algorithm locates the nearest neighbour (in Euclidean sense) to the initial point  $\{x(t_0), \dots, x(t_0 +$   
210  $(m - 1)\tau\}$  and denote the distance between these two points  $L(t_0)$ . At a later point  $t_1$ , the initial  
211 length will have evolved to length  $L'(t_1)$ . Then the MLE is calculated as:

212 
$$\lambda = \frac{1}{t_M - t_0} \sum_{k=1}^M \log_2 \frac{L'(t_k)}{L(t_{k-1})} \quad (7)$$

213  $M$  is the total number of replacement steps. We look for a new data point that satisfies two criteria  
214 reasonably well: its separation,  $L(t_1)$ , from the evolved fiducial point is small. If an adequate  
215 replacement point cannot be found, we retain the points that were being used. This procedure is  
216 repeated until the fiducial trajectory has traversed the entire data

217 **2.5 Approximate Entropy (ApEn)**

218 Approximate Entropy (ApEn) is one of the nonlinear dynamics tools that measure the dynamical  
219 complexity in observational time series. The concept was proposed by Pincus, (1991) which  
220 provides a generalized measure of regularity, such that it accounts for the logarithm likelihood in  
221 the observational time series. For instance, a dataset of length,  $N$ , that repeat itself for  $m$  points  
222 within a boundary will again repeat itself for  $m + 1$  points. Because of its computational

223 advantage, ApEn **has** been widely used in many areas of disciplines to study dynamical complexity  
224 (Pincus and Kalman (2004); Pincus and Goldberger (1994); McKinley et al. (2011); Kannathan et  
225 al. (2005); Balasis et al. (2009); Shujuan and Weidong, (2010); Moore and Marchant (2017)). The  
226 ApEn is computed using the formula below:

227 
$$ApEn(m, r, N) = \frac{1}{N-m+1} \sum_{i=1}^{N-m+1} \log C_i^m(r) - \frac{1}{N-m} \sum_{i=1}^{N-m} \log C_i^m(r) \quad (8)$$

228 where  $C_i^m(r) = \frac{1}{N-m+1} \sum_{j=1}^{N-m+1} \Theta(r - \|x_i - x_j\|)$  is the correlation integral,  $m$  is the embedding  
229 dimension and  $r$  is the tolerance. To compute the ApEn for the  $D_{st}$  and  $VB_s$  time series classified  
230 as minor, moderate and major geomagnetic storm from 2008 to 2016, we choose ( $m = 3, \tau =$   
231  $1hr$ ). We refer the works of Pincus, (1991); Kannathal et al. (2005); and Balasis et al. (2009) to  
232 interested readers where all the computational steps regarding ApEn were explained in details.  
233 Figures (5 & 6) depict the stem plot of ApEn for  $D_{st}$  and ( $VB_s$ ) from 2008 to 2016.

234 **2.6 Delay Vector Variance (DVV) analysis**

235 The Delay Vector Variance (DVV) is a unified approach in analyzing and testing for nonlinearity  
236 in a time series (Gautama et al. 2004; Mandic et al. 2007). The basic idea of the DVV is that, if  
237 two delay vectors of a predictable signal are close to each other in terms of the Euclidean distance,  
238 they should have similar target. For instance, when a time delay ( $\tau$ ) is embedded into a time series  
239  $x(k)$ ,  $k = 1, 2, \dots, N$ , then a reconstructed phase space vector is formed which represents a set of  
240 delay vectors (DVs) of a given dimension.

241 
$$X(k) = [X_{k-m\tau}, \dots, X_{k-\tau}]^T \quad (9)$$

242 Reconstructing the phase space, a set  $(\lambda_k)$  is generated by grouping those DVs that are with a  
243 certain Euclidean distance to DVs  $(X(k))$ . For a given embedding dimension  $(m)$ , a measure of  
244 unpredictability  $\sigma^2$  is computed over all pairwise Euclidean distance between delay vector as

245 
$$d(i, j) = \|x(i) - x(j)\| \quad (i \neq j) \quad (10)$$

246 Then, sets  $\lambda_k(r_d)$  are generated as the sets which consist of all delay vectors that lie closer to  $x(k)$   
247 than a certain distance  $r_d$ .

248 
$$\lambda_k(r_d) = \{x(i) \mid \|x(k) - x(i)\| \leq r_d\} \quad (11)$$

249 For every set  $\lambda_k(r_d)$ , the variance of the corresponding target  $\sigma^2$  ( $r_d$ ) is

250 
$$\sigma^2(r_d) = \frac{\frac{1}{N} \sum_{k=1}^N \sigma_k^2(r_d)}{\sigma_k} \quad (12)$$

251 where  $\sigma^2(r_d)$  is target variance against the standardized distance indicating that Euclidean  
252 distance will be varied in a manner standardized with respect to the distribution of pairwise  
253 distance between DVs. Iterative Amplitude Adjusted Fourier Transform (IAAFT) method is used  
254 to generate the surrogate time series (Kugiumtzis, 1999). If the surrogate time series yields DV  
255 plots similar to the original time series and the scattered plot coincides with the bisector line, then  
256 the original time series can be regarded as linear (Theiler et al. 1992; Gautama et al. 2004; Imitaz,  
257 2010; Jaksic et al. 2016). On the other hand, if the surrogate time series yield DV plot that is not  
258 similar to that of the original time series, then the deviation from the bisector lines indicates  
259 nonlinearity. The deviation from the bisector lines grows as a result of the degree of nonlinearity  
260 in the observational time series.

261

$$t^{DVV} = \sqrt{\langle (\sigma^{*2}(r_d) - \frac{\sum_{i=1}^N \sigma_{s,i}^{*2}}{N_s}) \rangle} \quad (13)$$

262 where  $\sigma_{s,i}^{*2}(r_d)$  is the target variance at the span  $r_d$  for the  $i^{th}$  surrogate. To carry out the test for  
263 nonlinearity in the  $D_{st}$  signals,  $m = 3$  and  $n_d = 3$ , the number of reference DVs=200, and number  
264 of surrogate,  $N_s = 25$  was used in all the analysis. Then we examined the nonlinearity response at  
265 minor, moderate and major geomagnetic storm.

266 **3.0 Results**

267 In this study,  $D_{st}$  and  $VB_s$  time series from January to December was analyzed for the period of  
268 nine years (2008 to 2016) to examine the chaotic and dynamical complexity response in the  
269 magnetospheric dynamics during **the month of** minor, moderate and major geomagnetic storms  
270 **activity**. Figures (1) & (2), display the samples of fluctuation signatures of  $D_{st}$  and  $VB_s$  signals  
271 classified as (a): **the month of** minor, (b): **the month of** moderate and (c): **the month of** major  
272 geomagnetic storm **activity**. The plot of Average Mutual information against time delay ( $\tau$ ) shown  
273 in Figure (3) depicts that the first local minimum of the AMI function was found to be roughly **at**  
274  $\tau = 15\text{hr}$ . Furthermore, we notice that the values of  $\tau$  near this value of ( $\sim 15\text{hr}$ ) maintain constancy  
275 for both  $VB_s$  and  $D_{st}$ . Also, in **Figure (4)**, we display the plot of **the percentage of false nearest**  
276 **neighbour** against embedding dimension ( $m$ ). It is obvious that a decrease in false nearest  
277 neighbour when increasing the embedding dimension drop steeply to zero at the optimal  
278 dimension( $m = 5$ ), thereafter the false neighbours stabilizes at that  $m = 5$  for  $VB_s$  and  $D_{st}$ .  
279 Therefore,  $m = 5$  and  $\tau = 15\text{hr}$  was used for the computation of MLE at different categories of  
280 geomagnetic storm, while  $m = 3$  and  $\tau = 1\text{hr}$  are applied for the computation of ApEn values.

281 The results of MLE (bar plot) and ApEn (stem plot) for  $D_{st}$  at **the month of** minor, moderate and  
282 major geomagnetic storms **activity** are shown in Figure 5. During **the month of** minor geomagnetic  
283 storms **activity**, we notice that the value of MLE ranges between 0.07 and 0.14 for most of the  
284 months classified as minor geomagnetic storm. Similarly, the ApEn (stem plot) ranges between  
285 **0.59 and 0.83**. It is obvious that strong chaotic behaviour with high dynamical complexity are  
286 associated with minor geomagnetic storms. During **the month of** moderate geomagnetic storm  
287 **activity**, (see b part of **Figure 5**), we observe a reduction in MLE values (0.04~0.07) compared  
288 to minor geomagnetic storm periods. Within the observed values of MLE during **the month of**

289 moderate geomagnetic storms **activity**, we found a slight rise of MLE in the following months  
290 (Mar 2008), (Apr 2011), (Jan 2012, Feb 2012, Apr 2012), (Jul 2015, Aug 2015, Sept 2015,  
291 Oct 2015, Nov 2015) and (Nov 2016). Also, the ApEn revealed a reduction in values between 0.44  
292 and 0.57 at **the month of moderate** geomagnetic storms **activity**. The lowest values of ApEn were  
293 noticed in the following months: May 2010, Mar 2011, and Jan 2016. During major geomagnetic  
294 storm as shown in Figure 5, the minimum and maximum value of MLE is respectively 0.03 and  
295 0.04 implying a very strong reduction of chaotic behaviour compared with **the month of minor** and  
296 moderate geomagnetic storm **activity**. The lowest values of MLE were found in the months of Jul  
297 2012, Jun 2013 and Mar 2015. Interestingly, further reduction in ApEn value (0.29~0.40) was as  
298 well noticed during this period. Thus, during **the month of** major geomagnetic storm **activity**,  
299 chaotic behaviour and dynamical complexity subsides significantly.

300 We display in Figure 6, the results of MLE and ApEn computation for the  $VB_s$  which has been  
301 categorized according to **the month of** minor, moderate and major geomagnetic storm **activity**. The  
302 values of MLE (bar plot) were between 0.06 and 0.20 for  $VB_s$ . The result obtained indicate strong  
303 chaotic behaviour with no significant difference in chaoticity during minor, moderate and major  
304 geomagnetic storm. Similarly, the results obtained from computation of ApEn (stem plot) for  $VB_s$   
305 depict a minimum value of 0.60 and peak value of 0.87 as shown in Figure 6. The ApEn values of  
306  $VB_s$  indicates high dynamical complexity response with no significant difference during the  
307 periods of the three categories of geomagnetic storm investigated.

308 The test for nonlinearity in the  $D_{st}$  signals during **the month of** minor, moderate and major  
309 geomagnetic storms **activity** was analyzed through the DVV analysis. Shown in Figure 9 is the  
310 DVV plot and DVV scatter plot during minor geomagnetic storm for January 2009 and January  
311 2014. We found that the DVV plots during **the month of** minor geomagnetic storms **activity** reveals

312 a slight separation between the original and surrogate data. Also, the DVV scatter plots shows a  
313 slight deviation from the bisector line between the original and surrogate data which implies  
314 nonlinearity. Also, during **the month of** moderate geomagnetic storm **activity**, we notice that the  
315 DVV plot depicts a wide separation between the original and the surrogate data. Also, a large  
316 deviation from the bisector line between the original and the surrogate data was also noticed in the  
317 DVV scatter plot as shown in Figure (8) thus indicating nonlinearity. In Figure (9), we display  
318 samples of DVV plot and DVV scatter plot during major geomagnetic storm for Oct 2011 and Dec  
319 2015. The original and the surrogate data showed a very large separation in the DVV plot during  
320 **the month of** major geomagnetic storm **activity**. While the DVV scatter plot depict the greatest  
321 deviation from the bisector line between the original and the surrogate data which is also an  
322 indication of nonlinearity. The DVV analysis of the  $VB_s$  time series during the **month of minor**,  
323 **moderate and major geomagnetic storm activity** shown in Figures (10-12) revealed a slight  
324 separation between the original and surrogate data with no significant difference between the  
325 **month of minor, moderate and major geomagnetic activity**.

326 **4.0 Discussion of Results**

327 **4.1 The chaotic and dynamical complexity response in  $D_{st}$  at minor, moderate and major**  
328 **geomagnetic storms**

329 Our result shows that the values of MLE for  $D_{st}$  during **the month of** minor geomagnetic storm  
330 **activity** are **higher**, indicating significant chaotic response during minor geomagnetic stormy  
331 periods (bar plot, Figure 5). This increase in chaotic behaviour for  $D_{st}$  signals during minor  
332 geomagnetic storm may be as a result of asymmetry features in the longitudinal distribution of  
333 solar source region for the Corotating Interaction Regions (CIR) signatures responsible for the  
334 development of geomagnetic storms (Turner et al. 2006; Kozyra et al. 2006). CIR generated

335 magnetic storms are generally weaker than ICME/MC generated storms (Richardson and Cane,  
336 2011). Therefore, we suspect that the increase in chaotic behaviour during minor geomagnetic  
337 storm is strongly associated with the asymmetry features in the longitudinal distribution of solar  
338 source region for the Corotating Interaction Regions (CIR) signatures. For most of these periods  
339 of moderate geomagnetic storms, the values of MLE decreases compared to **the month of** minor  
340 geomagnetic storms **activity**. This revealed that as geomagnetic stormy events build up, the level  
341 of unpredictability and sensitive dependence on initial condition (chaos) begin to decrease  
342 (Lorentz, 1963; Stogaz, 1994). The chaotic behaviour during **the month of** major geomagnetic  
343 storm decreases significantly compared with **the month of** moderate geomagnetic storm activity.  
344 The reduction in chaotic response during **the month of** moderate and its further declines at major  
345 geomagnetic storm **activity** may be attributed to the disturbance in the interplanetary medium  
346 driven by sheath preceding an interplanetary coronal mass ejection (ICME) or combination of the  
347 sheath and an ICME magnetic cloud (Echer et al. 2008; Tsurutani et al. 2003; Meng et al. 2019).  
348 Notably, the dynamics of the solar wind-magnetospheric interaction are dissipative chaotic in  
349 nature (Pavlos, 2012); and, the electrodynamics of the magnetosphere due to the flux of  
350 interplanetary electric fields had a significant impact on the state of the chaotic signatures. For  
351 instance, the observation of strong chaotic behaviour during **the month of** minor geomagnetic  
352 storm **activity** suggests that the dynamics was characterized by a weak magnetospheric  
353 disturbance. While the reduction in chaotic behaviour at moderate and major geomagnetic storm  
354 period reveals the dynamical features with regards to when a strong magnetospheric disturbance  
355 begins to emerge. Therefore, our observation of chaotic signatures at different categories of  
356 geomagnetic storm has potential capacity to give useful diagnostic **information about monitoring**  
357 space weather events. It is important to note that the features of  $D_{st}$  chaotic behaviour at different

358 categories of geomagnetic storm has not been reported in the literature. For example, previous  
359 study of Balasis et al. (2009, 2011) investigate dynamical complexity behaviour using different  
360 entropy measures and revealed the existence of low dynamical complexity in the magnetospheric  
361 dynamics and attributed it to ongoing large magnetospheric disturbance (major geomagnetic  
362 storm). The work of Balasis et al. (2009, 2011) where certain dynamical characteristic evolved in  
363 the  $D_{st}$  signal was revealed was limited to one year data (2001). It is worthy to note that the year  
364 2001, according to sunspot variations is a period of high solar activity during solar cycle 23. It is  
365 characterized by numerous and strong solar eruptions that were followed by significant magnetic  
366 storm activities. This confirms that on most of the days in year 2001, the geomagnetic activity is  
367 strongly associated with major geomagnetic storm. The confirmation of low dynamical complexity  
368 response in the  $D_{st}$  signal during major geomagnetic storm agree with our current study. However,  
369 the idea of comparing the dynamical complexity behaviour at different categories of geomagnetic  
370 storm and reveal its chaotic features was not reported. This is the major reason why our present  
371 investigation is crucial to the understanding of the level of chaos and dynamical complexity  
372 involved during different categories of geomagnetic storm. [As an extension to the single-year](#)  
373 [investigation](#) done by Balasis et al. (2009, 2011) during a major geomagnetic storm, we further  
374 investigated nine years data of  $D_{st}$  that covered minor, moderate and major geomagnetic storm  
375 (see [Figure 5](#), stem plots) and unveiled their dynamical complexity behaviour. During major  
376 geomagnetic stormy periods, we found that the ApEn values decrease significantly, indicating  
377 reduction in the dynamical complexity behaviour. This is in agreement with the low dynamical  
378 complexity reported by Balasis et al. (2009, 2011) during a major geomagnetic period. Finally,  
379 based on the method of DVV analysis, we found that test of nonlinearity in the  $D_{st}$  time series  
380 during major geomagnetic storm reveals the strongest nonlinearity features.

381 **4.2 The chaotic and dynamical complexity behaviour in the  $VB_s$  as input signals.**

382 The results of the MLE values for  $VB_s$  revealed a strong chaotic behaviour during the three  
383 categories of geomagnetic storm. Comparing these MLE values during **the month of** minor to those  
384 observed during moderate and major geomagnetic storm **activity**, the result obtained did not  
385 indicate any significant difference in chaoticity (bar plots, Figure 6). Also, the ApEn values of  
386  $VB_s$  during the periods associated with minor, moderate and major geomagnetic storm revealed  
387 high dynamical complexity behaviour with no significant difference between the three categories  
388 of geomagnetic storm investigated. These observation of high chaotic and dynamical complexity  
389 behaviour in the dynamics of  $VB_s$  may be due to interplanetary discontinuities **caused** by the abrupt  
390 changes in the interplanetary magnetic field direction and plasma parameters (Tsurutani et al.  
391 2010). Also, the indication of high chaotic and dynamical complexity behaviour in  $VB_s$  signifies  
392 that the solar wind electric field is stochastic in nature. **The DVV analysis for**  $VB_s$  **revealed**  
393 **nonlinearity features with no significant difference between the month of** minor, moderate and  
394 **major geomagnetic storm activity.** It is worth mentioning that the dynamical complexity behaviour  
395 for  $VB_s$  is different from what was observed for  $D_{st}$  time series data. For instance, our results for  
396  $D_{st}$  times series revealed that the chaotic and dynamical complexity behaviour of the  
397 magnetospheric dynamics are high during minor geomagnetic storm, reduce at moderate  
398 geomagnetic storm and further decline during major geomagnetic storm. While the  $VB_s$  signal  
399 revealed a high chaotic and dynamical complexity behaviour at all the categories of geomagnetic  
400 storm period. Therefore, these dynamical features obtained in the  $VB_s$  as input signal and the  $D_{st}$   
401 as the output in describing the magnetosphere as a non-autonomous system further support the  
402 finding of Donner et al. (2019) that found increased or not changed in dynamical complexity  
403 behaviour for  $VB_s$  and low dynamical complexity behaviour during storm using recurrence

404 method. Thus, suggesting that the magnetospheric dynamics is nonlinear and the solar wind  
405 dynamics is consistently stochastic in nature.

406 **5.0 Conclusions**

407 This work has examined the magnetospheric chaos and dynamical complexity behaviour in the  
408 disturbance storm time ( $D_{st}$ ) and solar wind electric field ( $VB_s$ ) as input during different categories  
409 of geomagnetic storm. The chaotic and dynamical complexity behaviour at **the month of** minor,  
410 moderate and major geomagnetic storm **activity** for solar wind electric field ( $VB_s$ ) as input and  
411  $D_{st}$  as output of the magnetospheric system were analyzed for the period of 9 years using nonlinear  
412 dynamics tools. Our analysis has shown a noticeable trend of these nonlinear parameters (MLE  
413 and ApEn) and the categories of geomagnetic storm (minor, moderate and major). The MLE and  
414 ApEn values of the  $D_{st}$  have indicated that the chaotic and dynamical complexity behaviour are  
415 high during **the month of** minor geomagnetic storm, low during moderate geomagnetic storm and  
416 further reduced during major geomagnetic storm **activity**. The values of MLE and ApEn obtained  
417 from  $VB_s$  indicate that chaotic and dynamical complexity are high with no significant difference  
418 during the **periods** of minor, moderate and major geomagnetic storm. Finally, the test for  
419 nonlinearity in the  $D_{st}$  time series during major geomagnetic storm reveals the strongest  
420 nonlinearity features. Based on these findings, the dynamical features obtained in the  $VB_s$  as input  
421 and  $D_{st}$  as output of the magnetospheric system suggest that the magnetospheric dynamics is  
422 nonlinear and the solar wind dynamics is consistently stochastic in nature.

423

424

425

426 **7.0 Acknowledgement**

427 The authors would like to acknowledge the World Data Centre for Geomagnetism, Kyoto, and the  
428 National Aeronautics and Space Administration, Space Physics Facility (NASA) for making the  
429 Dst data and solar wind plasma data available for research purpose.

430 **Declaration of Interest statement**

431 The authors declare that there is no conflicts of interest.

432 **References**

433 Baker, D.N., Klimas, A.J., (1990). The evolution of weak to strong geomagnetic activity: An  
434 interpretation in terms of deterministic chaos. *J. GeoPhys. Res. Letts.* Vol. 17, No. 1, PP. 41-  
435 44.

436 Balasis, G., Daglis, I.A., Anastasiadis, A., Eftaxias, K., (2011). Detection of dynamical complexity  
437 changes in Dst time series using entropy concepts and rescaled range analysis. W.Liu, M.  
438 Fujimoto (eds.), *The Dynamics Magnetosphere*, IAGA Special Sopron Book Series 3, doi:  
439 10.1007/978-94-007-0501-2\_12, Springer Science+Business Media B.V. 2011.

440 Balasis, G., I.A. Daglis, C. Papadimitriou, M. Kalimeri, A. Anastasiadis, K. Eftaxias (2009).  
441 Investigating dynamical complexity in the magnetosphere using various entropy measures,  
442 *J.Geophys.Res.*, 114, A0006, doi: 10.1029/2008JA 014035.

443 Balasis, G., I.A. Daglis, P. Kapiris, M.Mandea, D. Vassiliadis, K. Eftaxias (2006). From pre-storm  
444 activity to magnetic storms: a transition described in terms of fractal dynamics, *Ann.Geophys.*,  
445 24, 3557-3567, [www.ann-geophys.net/24/3557/2006](http://www.ann-geophys.net/24/3557/2006).

446 Balikhin, M.A., Boynton, R.J., Billings, S.A., Gedalin, M., Ganushkina, N., Coca, D., (2010). Data  
447 based quest for solar wind-magnetosphere coupling function, *Geophys.Res.Lett*, 37, L24107,  
448 doi: 10.1029/2010GL045733.

449 Burton, R.K., McPherron, R.L., Russell, C.T., (1975). An empirical relationship between  
450 interplanetary conditions and Dst. *Journal of Geophysical Research*, Vol.80, No.31.

451 Consolini, G., (2018), Emergence of dynamical complexity in the Earth's magnetosphere, Machine  
452 learning techniques for space weather, PP. 177-202, doi: 10.1016/B978-0-12-811788-0.00007-  
453 X

454 Cowley, S.W.H., (1995). The earth's magnetosphere: A brief beginner's guide, *EOS*  
455 *Trans.Am.GeoPhys.Union*, 76, 525.

456 Dessler, A.J., Parker, E.N., (1959). Hydromagnetic theory of magnetic storm. *J. GeoPhys. Res*, 64,  
457 PP 2239-2259.

458 Devi, S.P., Singh, S.B., Sharma, A.S., (2013). Deterministic dynamics of the magnetosphere:  
459 results of the 0-1 test. *Nonlin. Processes Geophys.*, 20, 11-18, 2013, [www.nonlin-processes-geophys.net/20/11/2013](http://www.nonlin-processes-geophys.net/20/11/2013), doi: 10.5194/npg-20-11-2013.

461 Donner, R.V., Balasis, G., Stolbova, V., Georgiou, M., Weiderman, M., Kurths, J. (2019).  
462 Recurrence-based quantification of dynamical complexity in the earth's magnetosphere at  
463 geospace storm time scales. *Journal of Geophysical Research: Space Physics*, 124, 90-108,  
464 doi: 10.1029/2018JA025318.

465 Echer, E., Gonzalez, D., Alves, M.V., (2006). On the geomagnetic effects of solar wind  
466 interplanetary magnetic structures. Space Weather, Vol.4, S06001,  
467 doi:10.1029/2005SW000200.

468 Echer, E., Gonzalez, W.D., Tsurutani, B.T., Gonzalez, A. L. C., (2008), Interplanetary conditions  
469 causing intense geomagnetic storms ( $D_{st} \leq -100nT$ ) during solar cycle 23 (1996–2006), J.  
470 Geophys. Res., 113, A05221, doi:10.1029/2007JA012744.

471 Fraser, A.M., (1986). Using mutual information to estimate metric entropy, dimension and  
472 entropies in chaotic system, Springer-Verlag, 1986, PP: 82-91.

473 Fraser, A.M., Swinney, H.L., (1986). Independent coordinates for strange attractors from mutual  
474 information, Phys.Rev.A 33, 1134-1140.

475 Gautama, T., Mandic, D.P., Hulle, M.M.V., (2004). The delay vector variance method for detecting  
476 determinism and nonlinearity in time series. Physica D, 190, 167-176, doi:  
477 10.1016/j.physd.2003.11.001.

478 Gonzalez, W.D., Joselyn, J.A., Kamide, Y., Kroehl, H.W., Rostoker, G., Tsurutani, B.T.,  
479 Vasyliunas, V.M., (1994). What is a geomagnetic storm? J. Geophys. Res.: Space Physics,  
480 Vol. 99, issue A4, pg. 5771-5792, doi: 10.1029/93JA02867.

481 Gonzalez, W.D., Tsurutani, B.T., (1987). Criteria of interplanetary parameters causing intense  
482 magnetic storm ( $Dst < -100nT$ ). Planetary and Space Science,  
483 <https://ntrs.nasa.gov/search.jsp?R=198800068>.

484 Horne, R.H., Glauert, S.A., Meredith, N.P., Boscher, D., Maget, V., Heynderickx, D., and Pitcford,  
485 D. (2013). Space weather impacts on satellites and forecasting the Earths electron radiation  
486 belts with SPACECAST. *Space weather*, **11**, 169 - 186

487 Imtiaz, A., (2010). Detection of nonlinearity and stochastic nature in time series by delay vector  
488 variance method, *International journal of Engineering & Technology*, Vol. 10, No. 02.

489 Jaksic, V., Mandic, D.P., Ryan, K., Basu, B., Pakrashi V., (2016). A Comprehensive Study of the  
490 Delay Vector Variance Method for Quantification of Nonlinearity in dynamical Systems.  
491 *R.Soc.OpenSci.*, 2016: 3:150493, <http://dx.doi.org/10.1098/rsos.150493>.

492 Johnson, J.R., Wing, S., (2005), A solar cycle dependence of nonlinearity in magnetospheric  
493 activity. *J. Geophys. Res.*, **110**, A04211, doi: 10.1029/2004JA010638.

494 Kannathal, N., M.L. Choo, U. R. Acharya, P. K. Sadasivan (2005). Entropies for detecting of  
495 epilepsy in EEG, *Computer Methods and Programs in Biomedicine* (2005) **80**, 187-194,  
496 [www.intl.elsevierhealth.com/journals/cmpb](http://www.intl.elsevierhealth.com/journals/cmpb).

497 Kennel, M.B., R. Brown, H.D.I. Abarbanel (1992). Determining embedding dimension for phase-  
498 space reconstruction using a geometrical construction, *PHYSICAL REVIEW A*, Volume 45,  
499 Number 6.

500 Klimas, A.J., Vassiliadis, D., Baker. D.N., Roberts, D.A., (1996). The organized nonlinear  
501 dynamics of the magnetosphere. *J. GeoPhys. Res.* Vol.101, No. A6, PP 13089-13113.

502 Kozyra, J.U., Crowley, G., Emery, B.A., Fang, X., Maris, G., Mlynczak, M.G., Niciejewski, R.J.,  
503 Palo, S.E., Paxton, L.J., Randall, C.E., Rong, P.P., Russell, J.M., Skinner, W., Solomon, S.C.,  
504 Talaat, E.R., Wu, Q., Yee, J.H., (2006), Response of the Upper/Middle Atmosphere to Coronal

505        **Holes and Powerful High-Speed Solar Wind Streams in 2003, Geophysical Monograph Series**  
506        **167, 10.1029/167GM24.**

507        Kugiumtzis, D., (1999). Test your surrogate before you test your nonlinearity, *Phys. Rev. E*, 60,  
508        2808-2816.

509        Lorenz, E.N., (1963). Determining nonperiodic flow. *J. Atmos.Sci.*,20,130.

510        Love, J.J., Gannon, J.L. (2009). Revised Dst and the epicycles of magnetic disturbance: 1958-2007.  
511        *Ann.GeoPhys.*, 27, 3101-3131.

512        Mandic, D.P., Chen, M., Gautama, T., Van Hull, M.M., Constantinides, A., (2007). On the  
513        Characterization of the Deterministic/Stochastic and Linear/Nonlinear Nature of Time Series.  
514        *Proc.R.Soc*, 2008: A464, 1141-1160, doi: 10.1098/rspa. 2007.0154.

515        Mane, R., (1981). On the dimension of the compact invariant sets of certain nonlinear maps, D.Rand  
516        and L.S.Young, eds, 1981.

517        Mckinley, R.A., McIntire, L.K., Schmidt, R., Repperger, D.W., Caldwell, J.A., (2011). Evaluation  
518        of Eye Metrics as a Detector of Fatigue. *Human factor*, 53 (4): 403-414, doi:  
519        10.1177/0018720811411297.

520        Mendes, O., Dominques, M.O., Echer, E., Hajra, R., Menconi, V.E., (2017), Characterization of  
521        high-intnesity, long-duration continuous auroral activity (HILDCAA) events using  
522        recurrence quantification analysis. *Nonlin. Processes Geophys.*,24,407-417, doi:10.5194/npg-  
523        24-407-2017.

524 Meng, X., Tsurutani, B. T., Mannucci, A. J. (2019). The solar and interplanetary causes of  
525 superstorms (minimum Dst  $\leq -250$  nT) during the space age. *Journal of Geophysical Research:*  
526 *Space Physics*, 124, 3926–3948. <https://doi.org/10.1029/2018JA026425>.

527 Millan, H., Gharbarian-Alavijeh, B., Garcia-Fornaris, I., (2010). Nonlinear dynamics of mean daily  
528 temperature and dewpoint time series at Babolsar, Iran, 1961-2005. Elsevier, *Atmospheric*  
529 *Research* 98 (2010) 89-101, doi: 10.1016/j.atmosres.2010.06.001.

530 Moore, C., Marchant, T., (2017). The approximate entropy concept extended to three dimensions  
531 for calibrated, single parameter structural complexity interrogation of volumetric images.  
532 *Physics in Medicine & Biology*, 62(15).

533 Oludehinwa, I.A., Olusola, O.I., Bolaji, O.S., Odeyemi, O.O., (2018). Investigation of nonlinearity  
534 effect during storm time disturbance, *Adv. Space. Res.*, 62 (2018) 440-456, doi:  
535 10.1016/j.asr.2018.04.032.

536 Omkar, P.T., Verma, P.L., (2013). Solar features and solar wind plasma parameters with  
537 geomagnetic storms during the period of 2002-2006. *Indian Journal of Applied Research*,  
538 Vol.3, Issue.5, ISSN-2249-555X.

539 Pavlos, G.P., (1994). The magnetospheric chaos: a new point of view of the magnetospheric  
540 dynamics. Historical evolution of magnetospheric chaos hypothesis the past two decades.  
541 Conference Proceeding of the 2nd Panhellenic Symposium held in Democritus University of  
542 Thrace, Greece, 26-29, April, edited 1994.

543 Pavlos, G.P., (2012). Magnetospheric dynamics and Chaos theory

544 Pavlos, G.P., Athanasiu, M.A., Diamantidis, D., Rigas, A.G., Sarri, E.T., (1999). Comments and  
545 new results about the magnetospheric chaos hypothesis. *Nonlinear Processes in Geophysics*  
546 (1999) 6: 99-127.

547 Pavlos, G.P., Rigas, A.G., Dialetis, D., Sarris, E.T., Karakatsanis, L.P., Tsonis, A.A., (1992).  
548 Evidence of chaotic dynamics in the outer solar plasma and the earth magnetosphere. *Chaotic*  
549 *dynamics: Theory and Practice*, Edited by T. Bountis, Plenum Press, New York, Page. 327-  
550 339, doi:10.1007/978-1-4615-3464-8\_30.

551 Pincus, S.M., (1991). Approximate entropy as a measure of system complexity, *Proc.Natl.Acad.Sci.*  
552 USA, Vol.88, PP. 2297-2301.

553 Pincus, S.M., Goldberger, A.L., (1994). Physiological time series analysis: what does regularity  
554 quantify, *The American Journal of Physiology*, 266 (4): 1643-1656.

555 Pincus, S.M., Kalman, E.K., (2004). Irregularity, volatility, risk, and financial market time series,  
556 *Proceedings of the National Academy of Sciences*, 101 (38): 13709-13714, doi:  
557 10.1073/pnas.0405168101.

558 Price, C.P., Prichard, D., Bischoff, J.E., (1994). Nonlinear input/output analysis of the auroral  
559 electrojet index. *Journal of Geophysical Research*, Vol.99, No: A7, PP: 227-238.

560 Price,C.P., Prichard, D., (1993). The Non-linear response of the magnetosphere: 30 October, 1978.  
561 *Geophysical Research Letters*, Vol.20.

562 Richardson, I.G., Cane, H.V., (2011), Geoeffectiveness ( $D_{st}$  and  $K_p$ ) of interplanetary coronal  
563 mass ejections during 1995-2009 and implication for storm forecasting, *Space Weather*, 9,  
564 S07005, doi:10.1029/2011SW000670.

565 Russell, C.T., (2001). Solar wind and Interplanetary Magnetic Field: A Tutorial. Space Weather,  
566 Geophysical Monograph 125, Page: 73-89.

567 Russell, C.T., McPherron, R.L., Burton, R.K. (1974). On the cause of geomagnetic storms,  
568 J.GeoPhys.Res., 79, 1105-1109.

569 Shujuan G., Weidong, Z., (2010). Nonlinear feature comparison of EEG using correlation  
570 dimension and approximate entropy, 3rd international conference on biomedical engineering  
571 and informatics.

572 Strogatz, S.H., (1994), Nonlinear dynamics and chaos with Application to physics, Biology,  
573 chemistry and Engineering, New York, John Wiley & Sons.

574 Sugiura, M. (1964). Hourly Values of equatorial Dst for the IGY, Ann.Int. GeoPhys. Year, 35, 9-  
575 45.

576 Takens, F., (1981). Detecting Strange Attractors in Turbulence in Dynamical Systems, D.Rand &  
577 L.Young Eds, 1981: 898, 366-381.

578 Theiler, J., Eubank, S., Longtin, A., Galdrikian, B., Farmer, J.D., (1992), Testing for nonlinearity  
579 in time series: The method of surrogate data, Physica D, 58, 77.

580 Tsurutani, B.T., Gonzalez, W. D., Tang, F., Akasofu, S.I., Smith, E.J., (1988), Origin of  
581 Interplanetary Southward Magnetic Fields Responsible for Major Magnetic Storms Near Solar  
582 Maximum (1978-1979), Journal of Geophysical Research, Vol. 93, No. A8, Pages 8519-8531,  
583 Paper number 7A9404, 0148-0227/88/007 A-9404\$05.00.

584 Tsurutani, B.T., Gonzalez, W.D., Lakhina, G.S. Alex, S., (2003). The extreme magnetic storm of  
585 1-2 September 1859, J. Geophys. Res. 108(A7), doi: 10.1029/2002JA009504.

586 Tsurutani, B.T., Lakhina, G.S., Hajra, R., (2020), The physics of space weather/solar-terrestrial  
587 physics (STP): what we know now and what the current and future challenges are, Nonlin.  
588 Processes Geophys., 27, 75–119, [doi:10.5194/npg-27-75-2020](https://doi.org/10.5194/npg-27-75-2020).

589 Tsurutani, B.T., Lakhina, G.S., Verkhoglyadova, O.P., Gonzalez, W.D., Echer, E., Guarnieri, F.L.,  
590 (2010). A review of interplanetary discontinuities and their geomagnetic effects. Journal of  
591 Atmospheric and Solar-Terrestrial Physics, doi: 10.1016/j.jastp.2010.04.001.

592 Tsutomu, N., (2002). Geomagnetic storms. Journal of communications Research Laboratory, Vol.  
593 49, No.3.

594 Turner, N.E., Mitchell, E.J., Knipp, D.J., Emery, B.A., (2006), Energetics of magnetic storms  
595 driven by corotating interaction regions: a study of geoeffectiveness, Geophysical Monograph  
596 Series 167, 10.1029/167GM11.

597 Unikrishnan, K., (2008). Comparison of chaotic aspect of magnetosphere under various physical  
598 conditions using AE index time series. Ann. Geophys., 26, 941-953, [www.ann-geophys.net/26/941/2008](http://www.ann-geophys.net/26/941/2008).

600 Unikrishnan, K., Ravindran, S., (2010). A study on chaotic behaviour of equatorial/low latitude  
601 ionosphere over indian sub-continent, using GPS-TEC time series, J. Atmos. Sol. Ter. Phys.,  
602 72, 1080-1089.

603 Valdivia, J.A., Rogan, J., Munoz, V., Gombertoff, L., Klimas, A., Vassiliadis, D., Uritsky, V.,  
604 Sharma, S., Toledo, B., Wastaviono, L. (2005). The magnetosphere as a complex system. Adv.  
605 Space. Res, 35, 961-971.

606 Valdivia, J.A., Sharma, A.S., Papadopoulos, K., (1996). Prediction of magnetic storms by nonlinear  
607 models. *Geophysical Research Letters*, 23(21), 2899-2902, doi: 10.1029/96GL02828.

608 Vassiliadis, D., (2006). Systems theory for geospace plasma dynamics, *Rev.Geophys.*, 44, RG2002,  
609 doi: 10.1029/2004RG000161.

610 Vassiliadis, D., Klimas, A.J., Valdivia, J.A., Baker, D.N., (1999). The geomagnetic response as a  
611 function of storm phase and amplitude and solar wind electric field. *Journal of Geophysical*  
612 *Research*, 104(A11), 24957-24976, doi: 10.1029/1999JA900185.

613 Vassiliadis, D., Sharma, A.S., Papadopoulos, K., (1991). Lyapunov exponent of magnetospheric  
614 activity from AL time series. *J. GeoPhys. Letts*, Vol. 18, No.8, PP. 1643-1646.

615 Vassiliadis, D.V., Sharma, A.S., Eastman, T.E., Papadopoulou, K., (1990). Low-dimensional  
616 chaos in magnetospheric activity from AE time series. *J. GeoPhys.Res.Lett*, 17, 1841-1844.

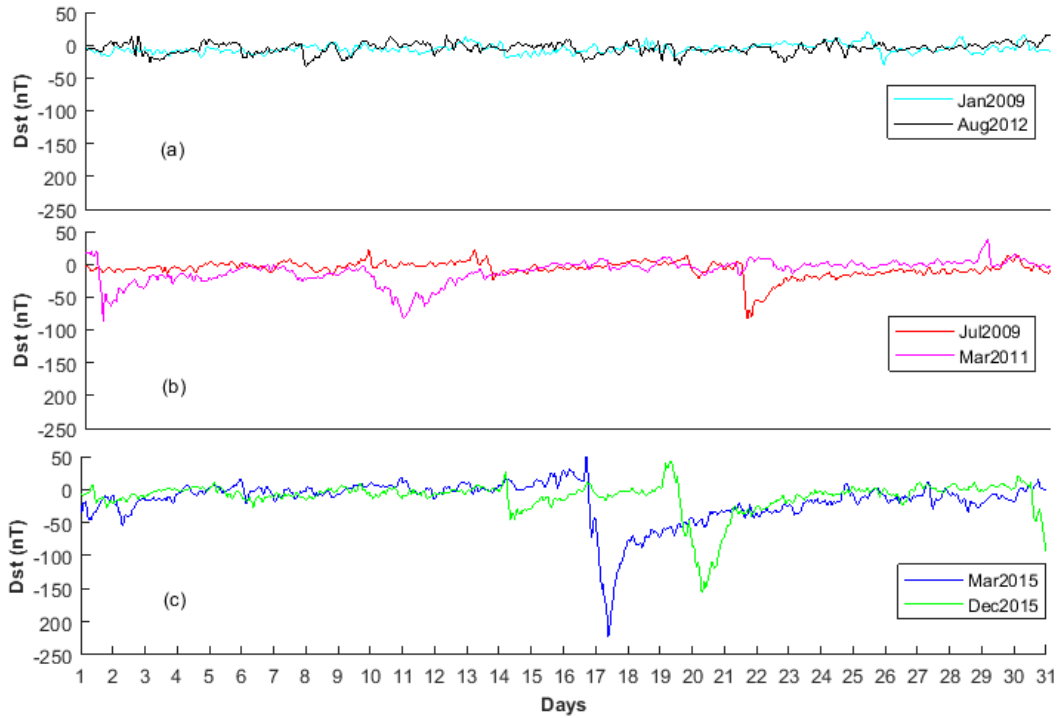
617 Wallot, S., Monster, D., (2018). Calculation of Average Mutual Information (AMI) and False  
618 Nearest Neighbours (FNN) for the estimation of embedding parameters of multidimensional  
619 time series in MATLAB. *Front. Physchol.* 9:1679, doi: 10.3389/fpsyg.2018.01679.

620 Watari, S., (2017). Geomagnetic storms of cycle 24 and their solar sources, *Earth, Planets and*  
621 *Space*, PP: 69:70, doi: 10.1186/s40623-017-0653-z.

622 Wolf, A., Swift, J. B., Swinney, H. L., and Vastano, J. A. (1985). Determining Lyapunov exponents  
623 from a time series, *Physica D*, 16, 285–317, doi:10.1016/0167-2789(85)90011-9.

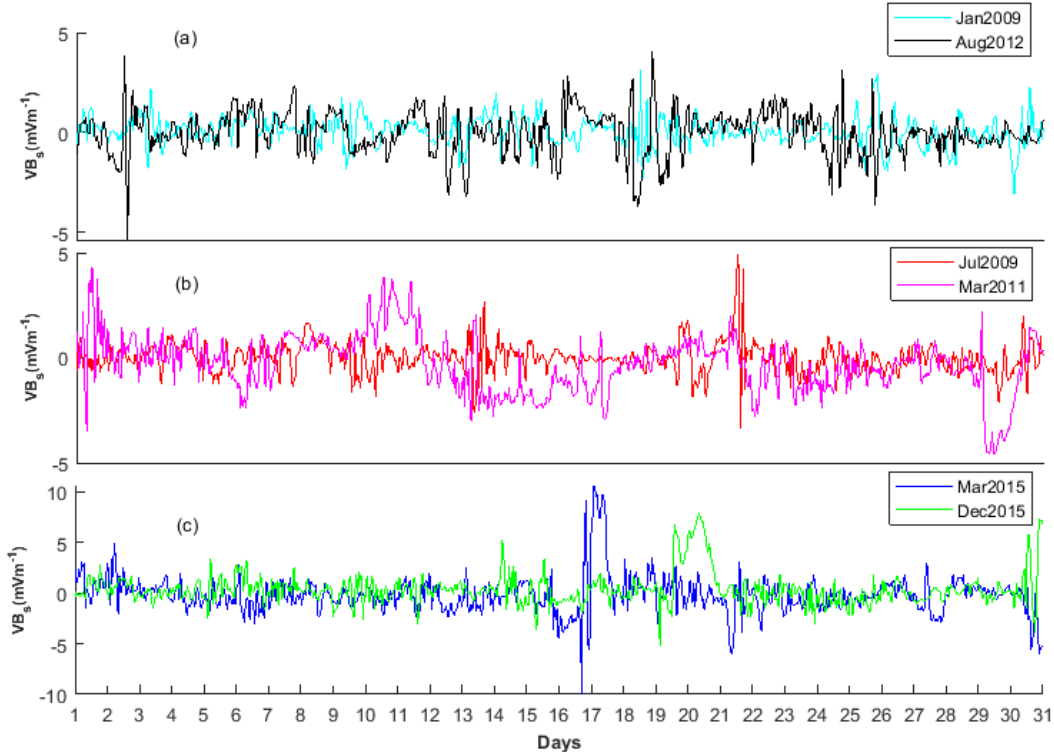
624 Zhang, J., Dere, K.P., Howard, R.A., Bothmer, V., (2002), Identification of solar sources of major  
625 geomagnetic storms between 1996 and 2000. *Astrophysical Journal*, 582:520-53.

626



627

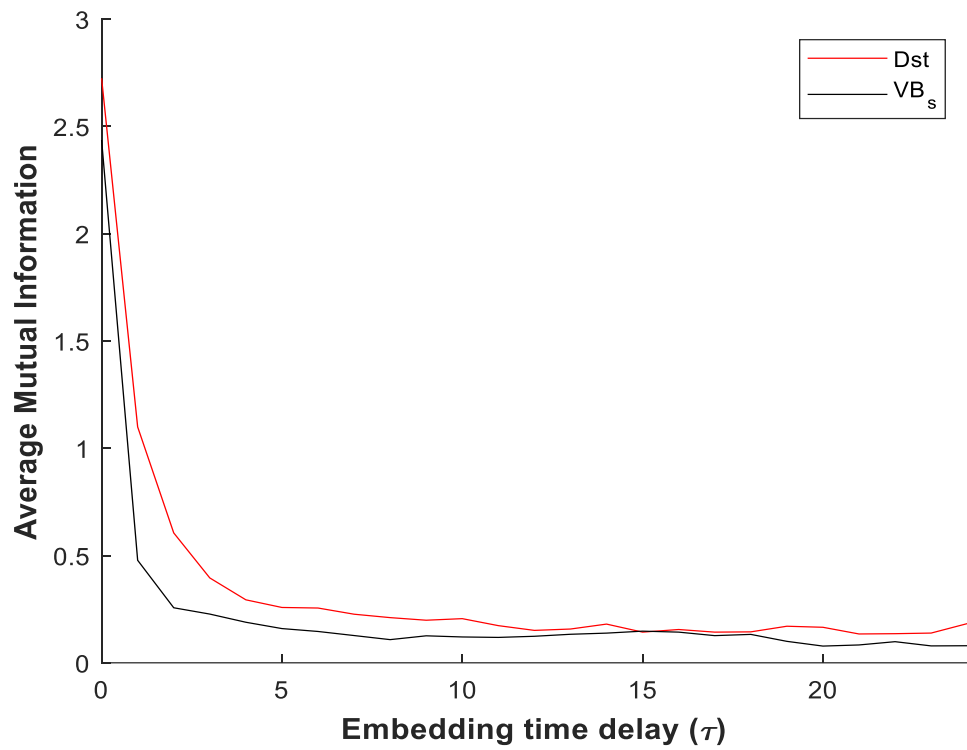
628 Figure 1: Samples of Dst signals classified as (a) Month of Minor, (b) Month of Moderate and (c)  
 629 Month of Major geomagnetic storm activity



630

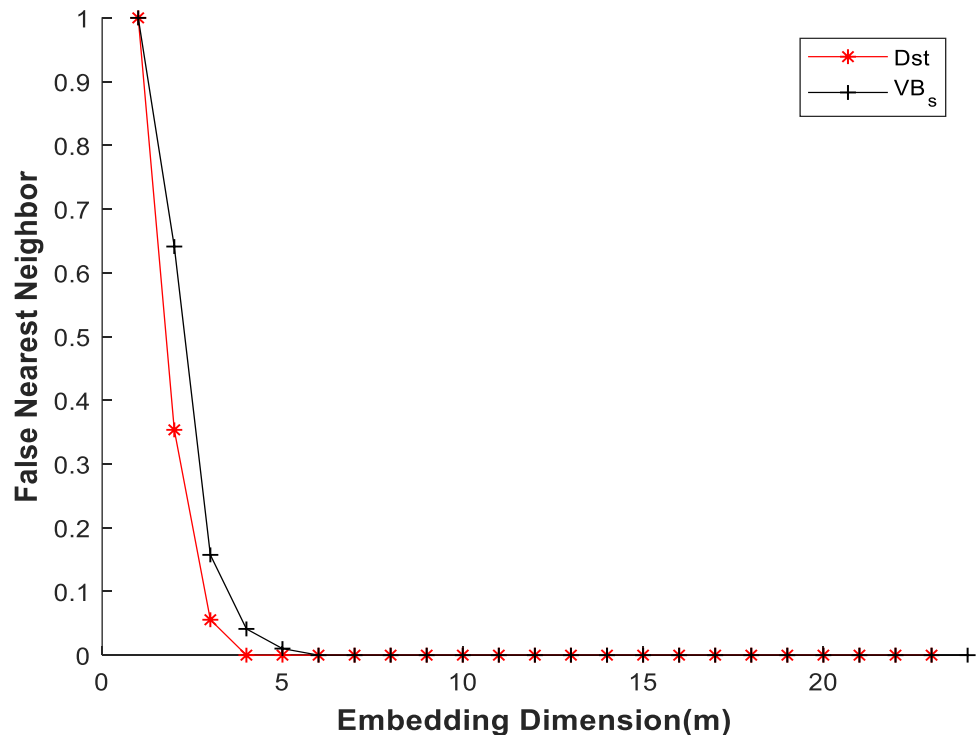
631 Figure 2: Samples of ( $VB_s$ ) during (a) Month of Minor, (b) Month of Moderate and (c) Month of  
 632 Major geomagnetic storm activity.

633



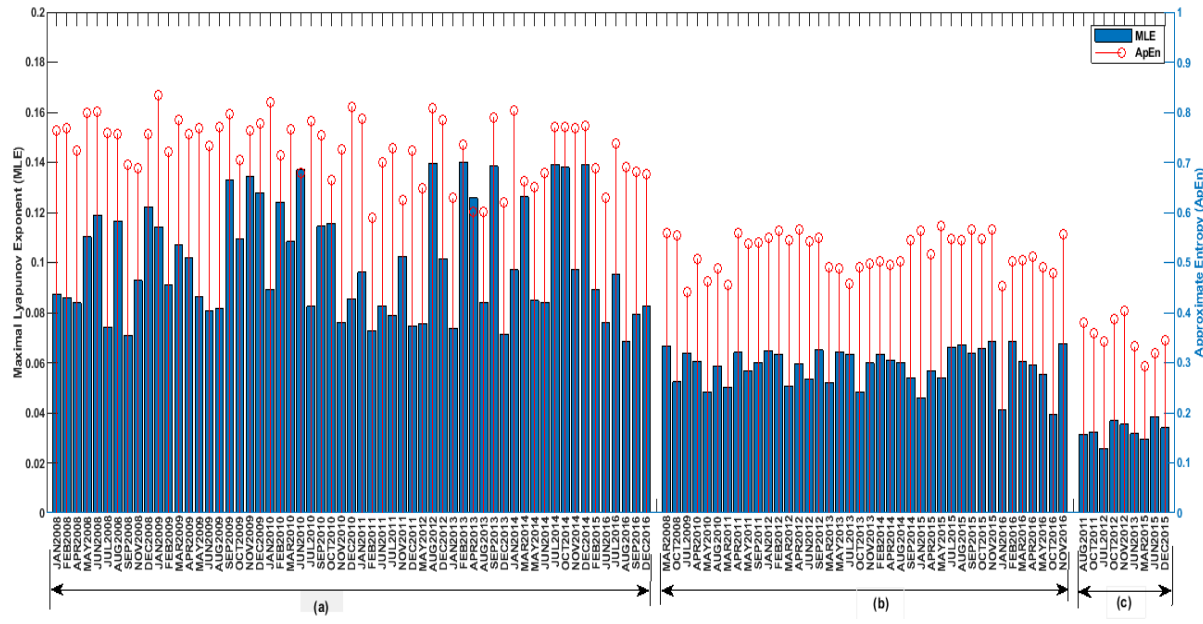
634

635 Figure 3: The plot AMI against embedding time delay ( $\tau$ )



636

637 Figure 4: The plot of FNN against embedding dimension (m)



638

639 Figure 5: The MLE (bar plot) and ApEn (stem plot) of Dst at: (a) Month of Minor, (b) Month of  
 640 Moderate and (c) Month of Major geomagnetic storm activity

641

642

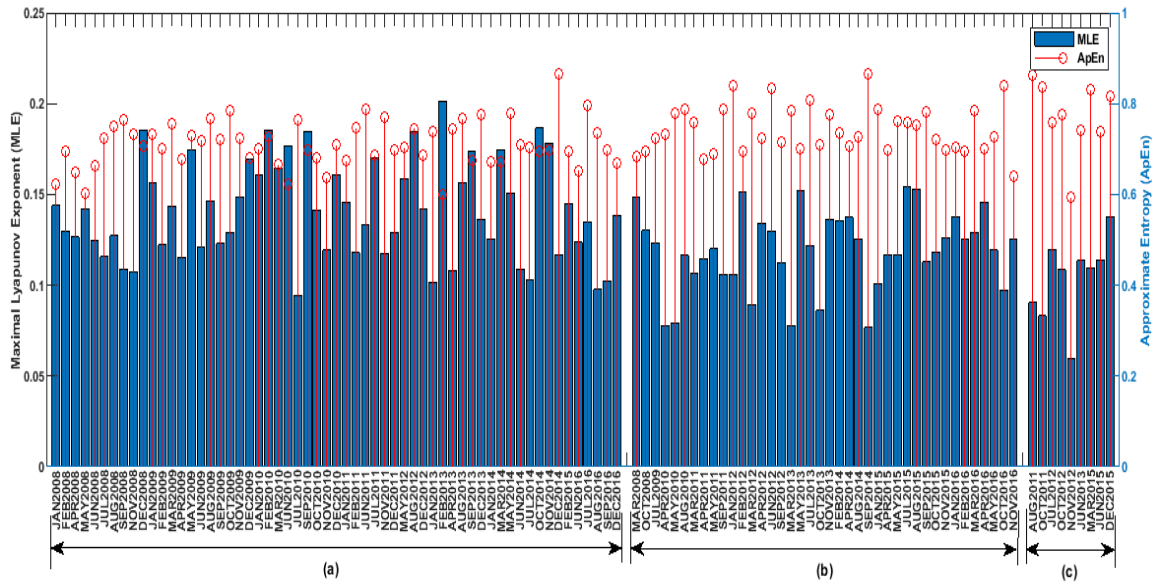
643

644

645

646

647



648

649 Figure 6: The MLE (bar plot) and ApEn (stem plot) of solar wind electric field ( $VB_s$ ) during: (a)  
650 **Month of Minor**, (b) **Month of Moderate** and (c) **Month of Major** geomagnetic storm **activity**.

651

652

653

654

655

656

657

658

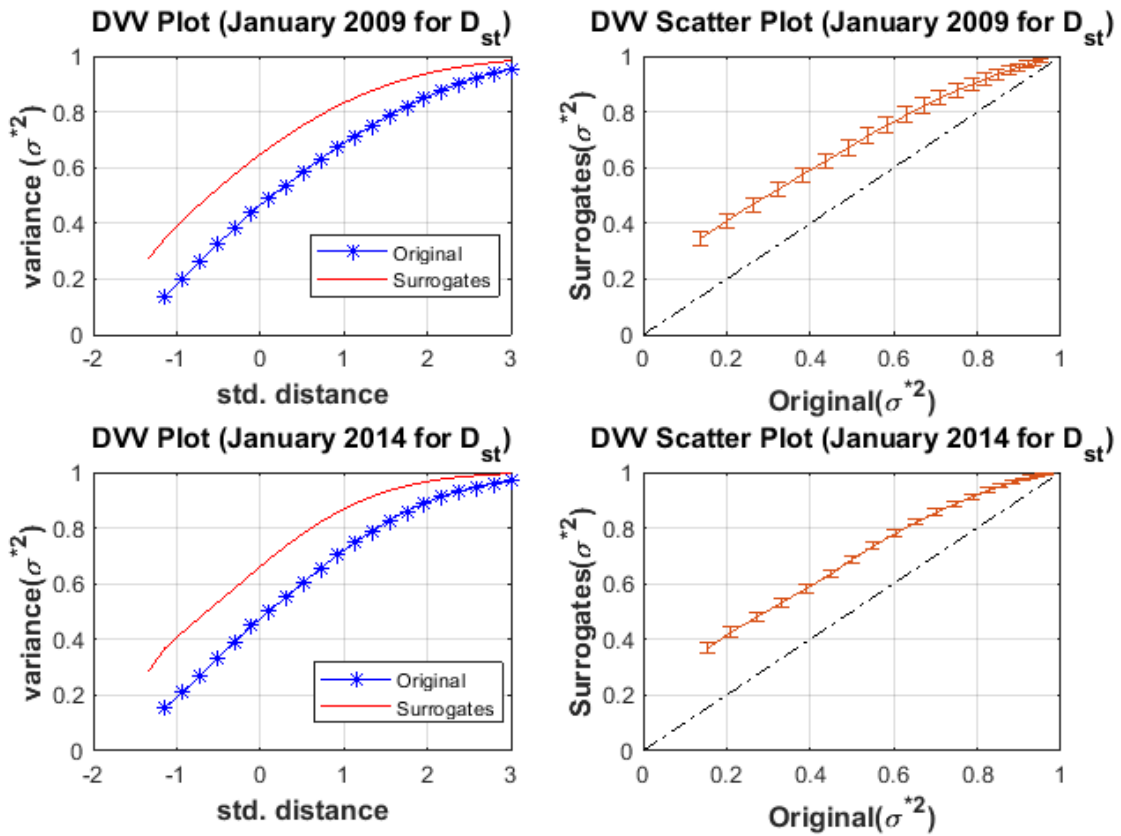
659

660

661

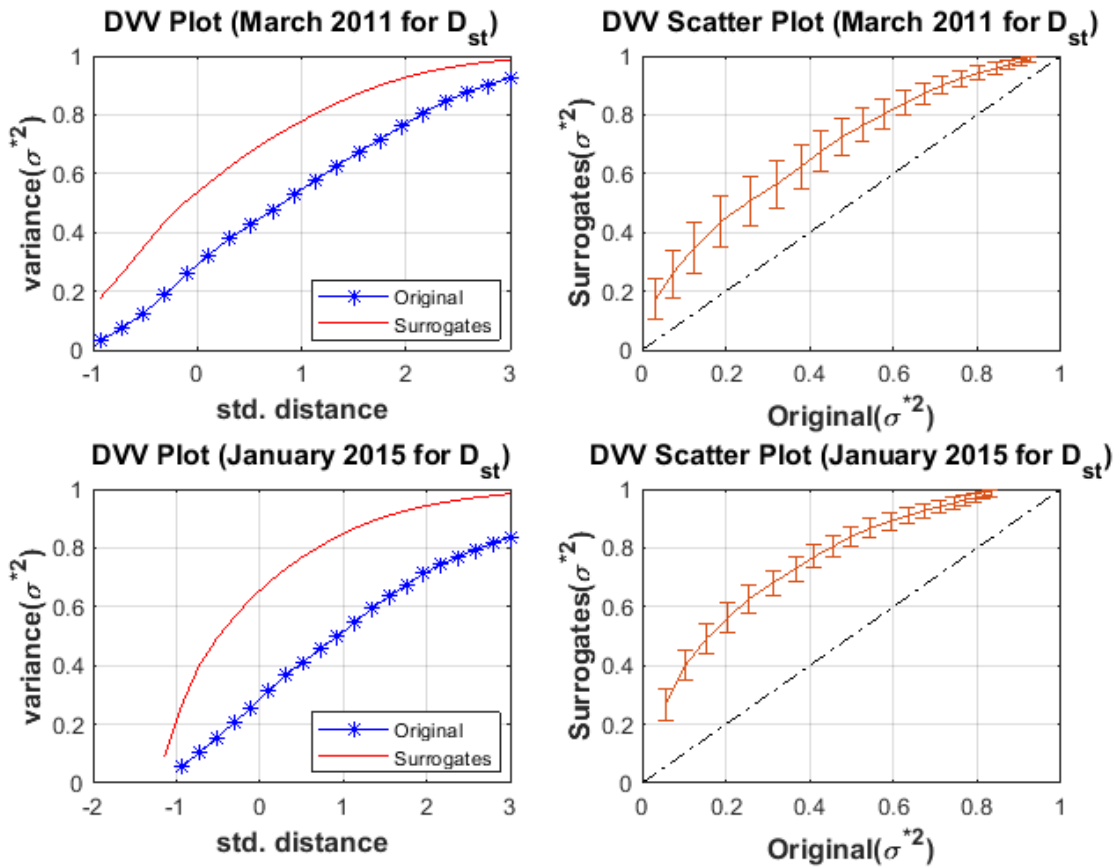
662

663



664

665 Figure 7: The DVV plot and Scatter plot for  $D_{st}$  during the month of minor geomagnetic storm  
 666 for January 2009 and January 2014.

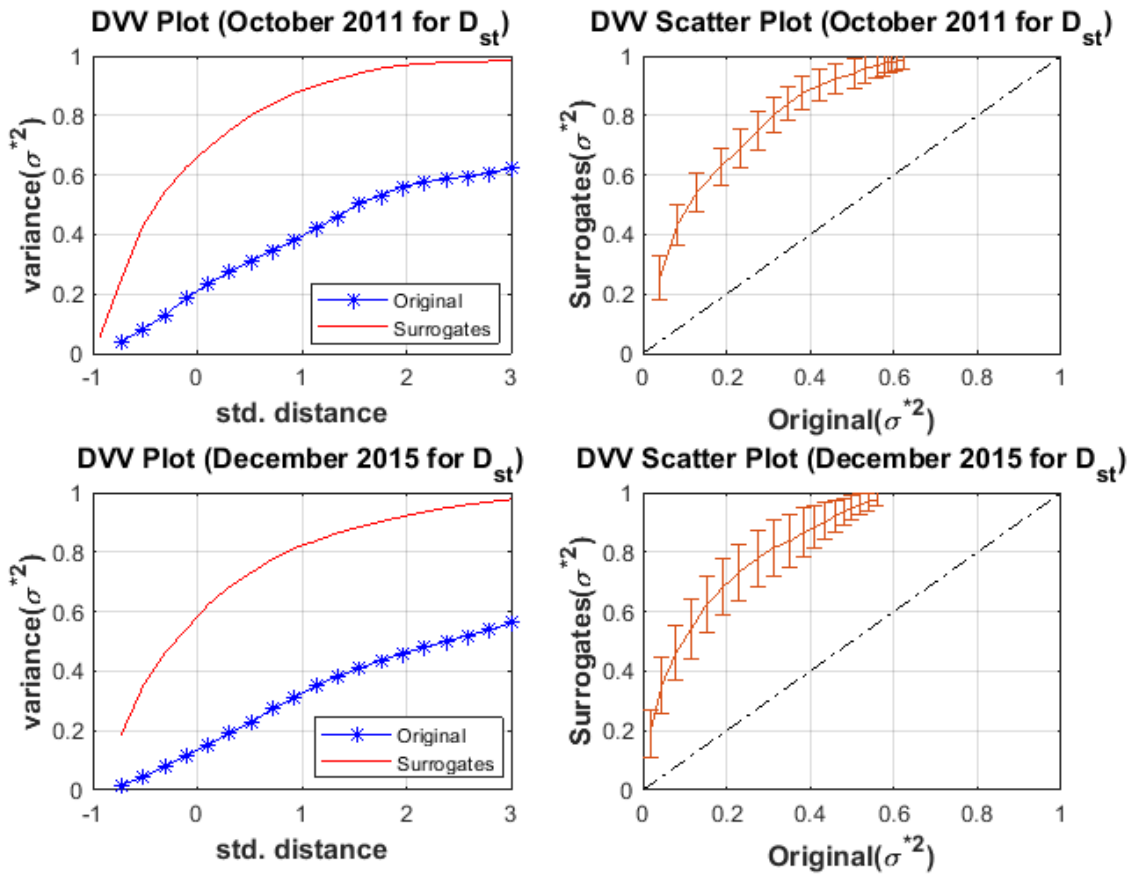


667

668

669 Figure 8: The DVV plot and Scatter plot for  $D_{st}$  during the month of moderate geomagnetic storm  
 670 for March 2011 and January 2015.

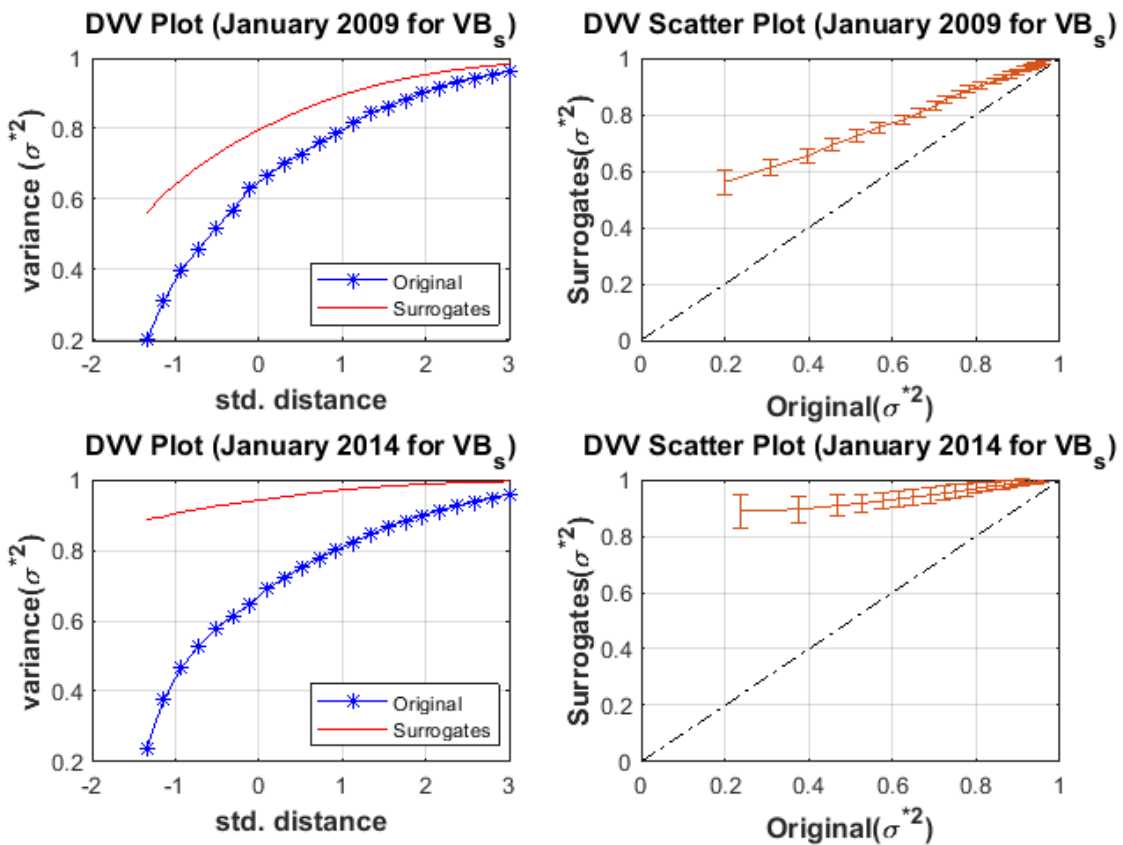
671



672

673 Figure 9: The DVV plot and Scatter plot for  $D_{st}$  during the month of major geomagnetic storm  
 674 for October 2011 and December 2015.

675

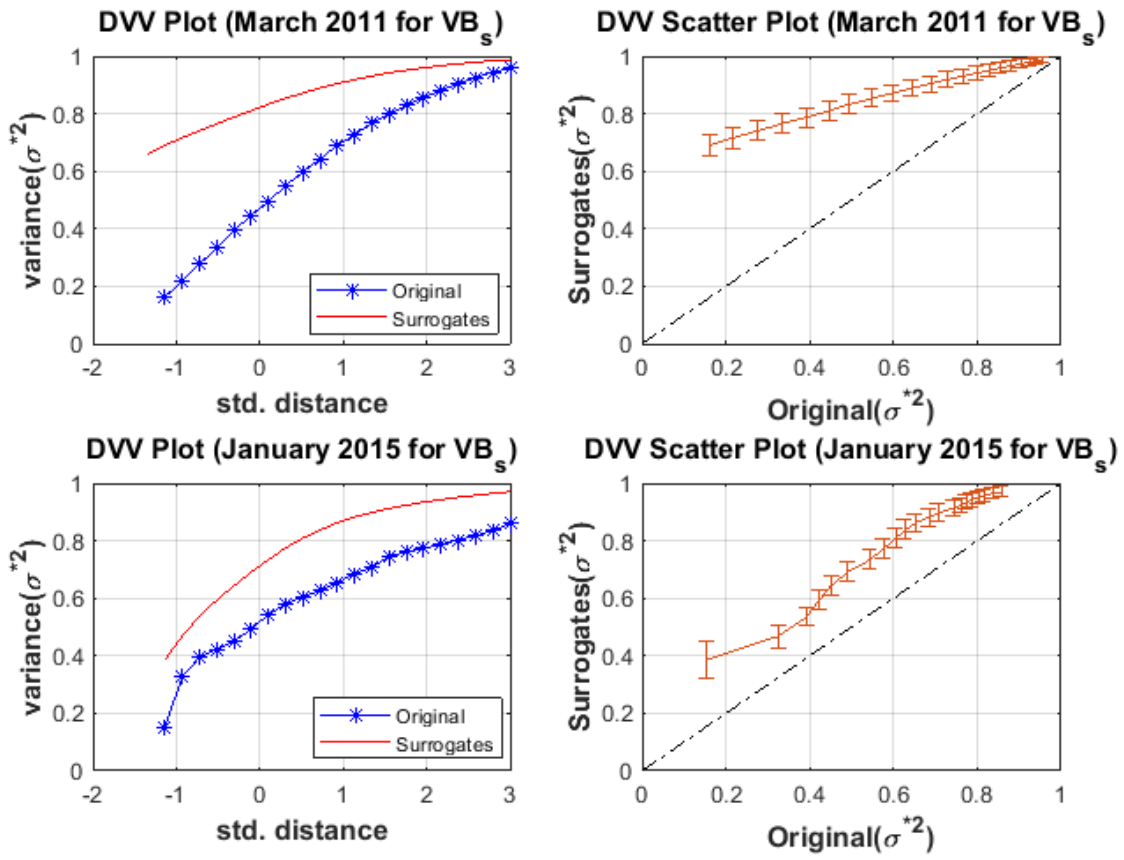


676

677 Figure 10: The DVV plot and Scatter plot for  $VB_s$  during the month of minor geomagnetic storm  
 678 for January 2009 and January 2014.

679

680

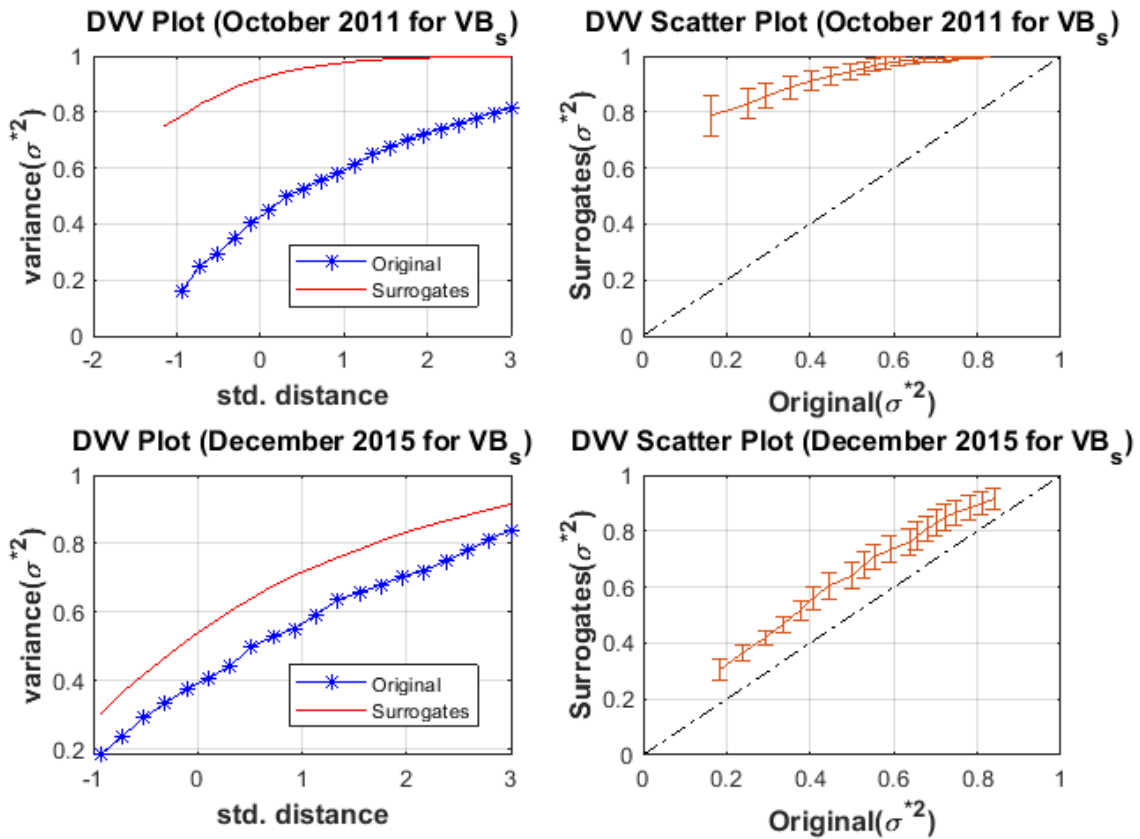


681

682 Figure 11: The DVV plot and Scatter plot for  $VB_s$  during the month of moderate geomagnetic  
 683 storm for March 2011 and January 2015.

684

685



686

687 Figure 12: The DVV plot and Scatter plot for  $VB_s$  during the month of major geomagnetic storm  
 688 for October 2011 and December 2015.

689

690

691